Journal of Nuclear Materials 405 (2010) 235–243

Contents lists available at ScienceDirect

Journal of Nuclear Materials

journal homepage: www.elsevier.com/locate/jnucmat

Raman spectroscopy characterization of actinide oxides $(U_{1-y}Pu_y)O_2$: Resistance to oxidation by the laser beam and examination of defects

C. Jégou [a,*], R. Caraballo [a], S. Peuget [a], D. Roudil [a], L. Desgranges [b], M. Magnin [a]

[a] Commissariat à l'Énergie Atomique (CEA/DEN/DTCD), Marcoule Research Center, 30207 Bagnols-sur-Cèze Cedex, France
[b] Commissariat à l'Énergie Atomique (CEA/DEN/DEC), Cadarache Research Center, 13108 Saint-Paul-lez-Durance Cedex, France

ARTICLE INFO

Article history:
Received 16 April 2010
Accepted 4 August 2010

ABSTRACT

Structural changes in four $(U_{1-y}Pu_y)O_2$ materials with very different plutonium concentrations ($0 \leqslant y \leqslant 1$) and damage levels (up to 110 dpa) were studied by Raman spectroscopy. The novel experimental approach developed for this purpose consisted in using a laser beam as a heat source to assess the reactivity and structural changes of these materials according to the power supplied locally by the laser. The experiments were carried out in air and in water with or without hydrogen peroxide. As expected, the material response to oxidation in air depends on the plutonium content of the test oxide. At the highest power levels U_3O_8 generally forms with UO_2 whereas no significant change in the spectra indicating oxidation is observed for samples with high plutonium content ($^{239}PuO_2$). Samples containing 25 wt.% plutonium exhibit intermediate behavior, typified mainly by a higher-intensity 632 cm^{-1} peak and the disappearance of the 1LO peak at 575 cm^{-1}. This can be attributed to the presence of anion sublattice defects without any formation of higher oxides. The range of materials examined also allowed us to distinguish partly the chemical effects of alpha self-irradiation. The results obtained with water and hydrogen peroxide (a water radiolysis product) on a severely damaged $^{238}PuO_2$ specimen highlight a specific behavior, observed for the first time.

© 2010 Elsevier B.V. All rights reserved.

1. Introduction

Mixed $(U,Pu)O_2$ actinide oxides are widely used in the nuclear industry, and it is therefore essential to understand their oxidation processes. From fuel fabrication to spent fuel management these oxides can be subjected to various media (air, water, steam, etc.) that can affect their reactivity and/or accelerate their corrosion. Despite their identical crystal structure (cubic fluorite structure, Fm-3m space group), UO_2 and PuO_2 exhibit very different oxidation behavior. This subject has been widely investigated and discussed in recent years [1–10]. A recent explanation is based on the relative position of the 5*f* electrons with respect to the O 2*p* band. Oxidation is energetically favorable if this band is situated below the 5*f* levels, as in the case of UO_2; conversely, oxidation is no longer possible if the levels overlap (as for PuO_2) [3]. Nevertheless, some doubt remains concerning the oxidation of plutonium under water radiolysis, as these energy levels can be reversed. Calculations [2] have shown that PuO_2 oxidation by H_2O_2 could be energetically favorable with the formation of Pu_4O_9 as an intermediate reaction product on the oxide surface. Moreover, in addition to the behavior of simple UO_2 and PuO_2 oxides, the oxidation resistance of $(U_{1-y}Pu_y)O_2$ solid solutions versus the plutonium concentration and matrix self-irradiation damage level is a fundamental subject of investigation. Recent work by Jégou et al. [11] showed that the plutonium concentration is an essential parameter affecting the oxidation resistance of spent MOX fuel subjected to water radiolysis.

Experimental techniques have also been developed in recent years to provide structural data in this area. One of these techniques is Raman spectroscopy. It can provide relevant data on the structural changes occurring on the surface of polycrystalline materials at cubic micrometer scale after correction for material behavior and changes under the laser beam, and in combination with other experimental techniques (especially X-ray diffraction, X-ray absorption, and SEM) [12–14]. This method has been successfully applied to UO_2 and its higher oxide forms UO_{2+x} to U_3O_8. He and Shoesmith [14] recently combined Raman spectroscopy with X-ray diffraction to study phase transitions and defects in hyperstoichiometric uranium oxides.

Raman spectroscopy is now available in high-activity laboratories [11]. We used it to investigate structural changes in four $(U_{1-y}Pu_y)O_2$ materials with very different plutonium content and damage levels. The novel experimental approach developed for this purpose consisted in using a laser beam as a heat source to assess the reactivity and structural changes of these materials

* Corresponding author. Address: Commissariat à l'Énergie Atomique (CEA), Marcoule Center, DTCD/SECM/LMPA, BP 17171, F-30207 Bagnols-sur-Cèze Cedex, France. Tel.: +33 466 791642; fax: +33 466 797708.
E-mail address: christophe.jegou@cea.fr (C. Jégou).

0022-3115/$ - see front matter © 2010 Elsevier B.V. All rights reserved.
doi:10.1016/j.jnucmat.2010.08.005

according to the power supplied locally by the laser. The experiments were carried out mainly in air and in water.

2. Experimental

2.1. Materials

Four materials with variable plutonium content and very different damage levels were examined in this study.

2.1.1. UO_2 pellets

UO_2 pellets were annealed in Ar + 4% H_2 for 10 h at 450 °C to restore their stoichiometry and constitute the control specimens (undamaged, unoxidized fluorite structure). The pellets were dense (geometric density 10.63 g cm^{-3}, or 97% TD) and were fabricated by sintering depleted uranium powder (^{235}U = 0.21 wt.%).

2.1.2. $(U,Pu)O_{2-x}$ pellets

UO_2 pellets doped with 25 wt.% plutonium were also tested. These homogeneous "Gigondas" ($(U,Pu)O_{2-x}$) solid solution) pellets were fabricated in 1985 at CEA Cadarache and have not been subjected to high-temperature annealing since that time. The initial mixed oxide stoichiometry was O/M = 1.983; the geometric density was 10.421 g cm^{-3} and the initial isotopic composition was as follows (wt.%): $^{238}Pu/Pu$ = 0.220; $^{239}Pu/Pu$ = 70.090; $^{240}Pu/Pu$ = 24.510; $^{241}Pu/Pu$ = 4.095; $^{242}Pu/Pu$ = 1.085; $^{235}U/U$ = 0.730; $^{238}U/U$ = 99.270. The isotopes responsible for the most of the alpha self-irradiation of these samples were ^{238}Pu and ^{241}Am, a β-decay

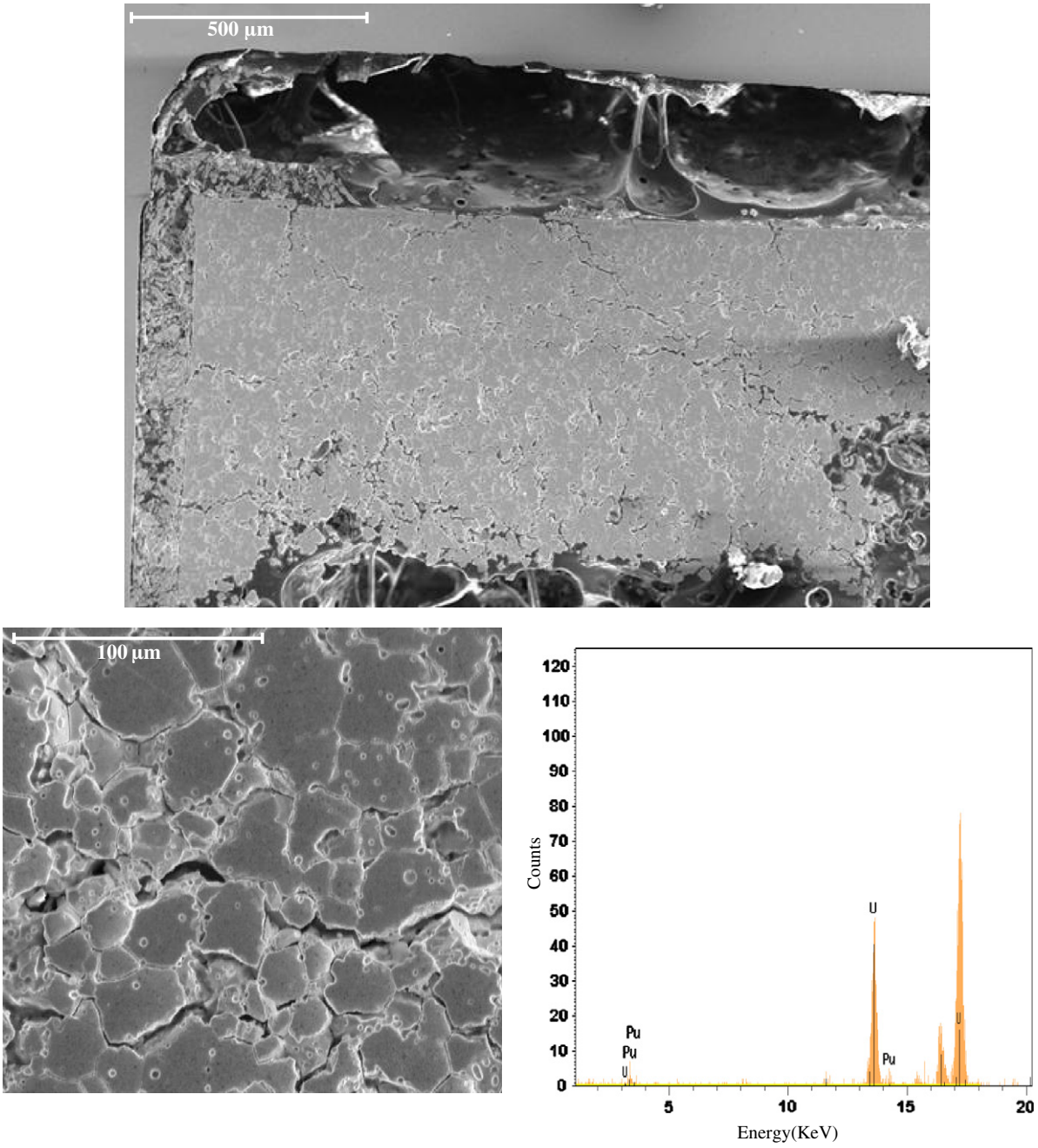

Fig. 1. Scanning electron micrograph of a radioisotope containing plutonium oxide ($^{238}PuO_2$) observed under standard analysis conditions (20 kV, working distance 15 mm). A characteristic spontaneous spectrum was obtained during analysis without the electron beam (indicating the presence of decay plutonium and uranium).

product of ^{241}Pu. The integrated dose after 25 years of interim storage was about 1.4×10^{18} α g^{-1}. Assuming each disintegration generates about 1500 atomic displacements [15] and excluding recombinations, the damage level is about 0.3 displacements per atom (dpa).

2.1.3. Plutonium-238 oxide ($^{238}PuO_2$) radioisotope source

Plutonium-238 oxide radioisotope sources were produced by the CEA between 1974 and 1976 [16] for use as energy sources in thermopile generators suitable for cardiac pacemakers. The sources comprise a pellet 4.2 mm in diameter and 1.7 mm high, inside a triple tantalum–platinum–tantalum encapsulation (Fig. 1). Before sintering, the powder was heat treated in oxygen depleted in ^{18}O to enhance ^{16}O–^{18}O isotopic exchange and thus considerably reduce neutron emissions by (α,*n*) reaction. At the moment of fabrication the pellet geometric density was 9.2 g cm^{-3} (i.e. about 85% TD). Today, 35 years later, these samples have reached a very high integrated α dose — about 5×10^{20} α g^{-1} corresponding to about 110 dpa — and contain 20 wt.% ^{234}U produced by alpha decay.

2.1.4. PuO_2 powder

The isotopic composition of the PuO_2 batch used for this study was as follows (in August 2002): ^{238}Pu/Pu = 0.07; ^{239}Pu/Pu = 66.17; ^{240}Pu/Pu = 29.20; ^{241}Pu/Pu = 1.53; ^{242}Pu/Pu = 3.03 wt.%. The batch was produced by plutonium oxalate precipitation followed by calcining of the oxalate in air for 10 h at 100 °C. Scanning electron microscopic observation of the plutonium oxide powder (Fig. 2a and b) revealed the presence of fine particles with a characteristic dimension of 2 μm (Fig. 2c) together with agglomerates measuring several tens of micrometers (Fig. 2d). Given its isotopic composition, the batch damage level batch is about 0.2 dpa, substantially less than that of the radioisotope sources. Moreover the ^{234}U content was very low, less than 0.04 wt.%. The sample chemical composition is interesting because its oxidation response can be assumed to be very limited; its morphology is also of interest here because powders are generally more reactive than solid samples [12].

2.2. Raman spectroscopy

A Jobin–Yvon LabRam Raman spectrometer was used in conjunction with a nuclearized microscope (Optique Peter, Lyon, France) with an objective turret (×1.25, ×5, ×10, ×20, ×50 and ×100). A YAG laser (532 nm) with output power adjustable from 50 to 110 mW was used with a variable filter to provide low excitation beam power levels.

The optical microscope is mounted in a hot cell, while the Raman spectrometer and laser are installed outside the cell with a fiber-optic signal transmission line. The instrument was verification and calibrated prior to use to ensure satisfactory acquisition of high-quality spectra. This procedure consisted first in adjusting the position of the CCD array with respect to the Raman return signal, then adjusting the zero-order beam reference setting for Raman shifts with respect to the incident laser wavelength. Wave number calibration was then performed on a silicon sample. The calibration coefficient was modified to position the main peak at the benchmark value of 520.4 cm^{-1}.

The laser generator and lens output power levels were measured using a Coherent LaserCheck® hand-held laser power meter comprising a silicon cell with an 8 mm aperture suitable for the wavelength of our laser (wavelength adjustment range: 400–1064 nm) and capable of measuring power levels ranging from 9.99 μW to 999 mW with ±5% accuracy. The device was fitted with provisions for use with a telemanipulator to allow hot-cell measurements at the microscope objective lenses. The measurement conditions for this study are detailed in Table 1. The sample surface was probed at three power levels: P_{max}, P_{min} and P_{min} + F3 using an attenuation filter. Raman spectra were acquired at these power settings or at P_{min} + F3 after heating the surface locally at P_{max} or

Table 1
Measured power output from the laser and from the objective lens in the hot cell.

	P_{max}	P_{min}	P_{min} + F3
Generator output power (mW)	110 ± 6	52 ± 3	8 ± 0.4
Objective lens output power (mW)	19 ± 1	9 ± 0.5	1.4 ± 0.1

Table 2
Laser power density (mW μm^2) versus laser power and objective lens.

	P_{max}	P_{min}	P_{min} + F3
Objective lens × 100	37 ± 2	17 ± 1	2.7 ± 0.2
Objective lens × 20	9 ± 0.5	4 ± 0.2	0.7 ± 0.05

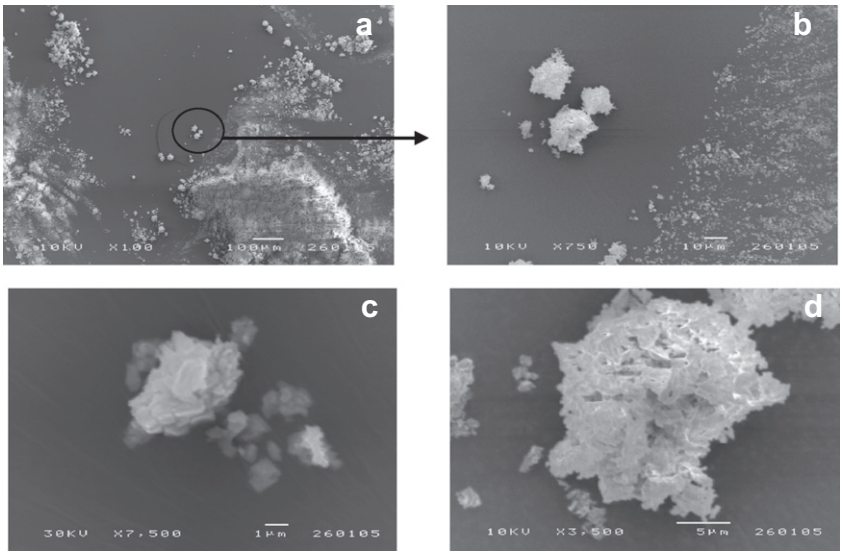

Fig. 2. $^{239}PuO_2$ powder morphology observed by scanning electron microscope.

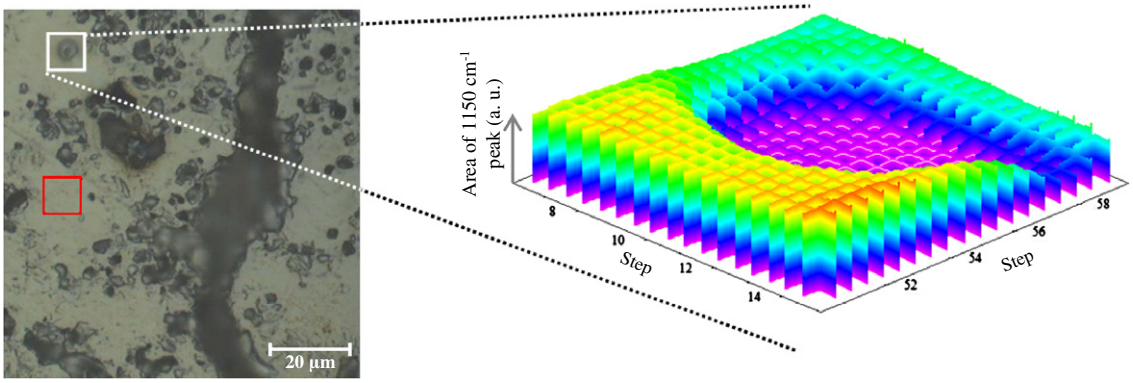

Fig. 3. Left: optical microscope image (×100) of UO_2 sample (scale: 20 µm). The laser impact at P_{max} was observed on the surface (white square). The red square indicates a zone probed by the laser at low power with an attenuation filter (P_{min} + F3). Right: Raman map (1150 cm^{-1} 2LO peak characteristic of UO_2) of impact zone (10 × 10 $µm^2$) to assess the degree of oxidation. Blue/pink areas represent highly oxidized zones (U_3O_8) and green/yellow areas correspond to unoxidized zones (UO_2). (For interpretation of the references to colour in this figure legend, the reader is referred to the web version of this article.)

P_{min}. For all the sintered pellets the laser was focused on the sample surface using the ×100 objective (0.5 $µm^2$ spot size). For the $^{239}PuO_2$ powder, however, the ×20 objective (2 $µm^2$ spot size) was used to prevent any interaction with the substrate and avoid damaging the highly reactive powder. The deposited laser power densities are indicated in Table 2. It is impossible to estimate the local temperatures because the experimental device installed in a shielded cell is equipped with edge filters that pass only one laser sideband: the Stokes or anti-Stokes component. A choice muse be made (Stokes component) that prevents calculation of local temperatures by comparing the Stokes and anti-Stokes intensities, for example.

3. Results and discussion

The oxidation resistance of the previously described actinide oxides was investigated by a novel experimental approach. The laser beam is used as a heat source to assess the reactivity, and structural changes in these materials are observed in the Raman spectra.

3.1. Experimental device qualification procedure

Tests were carried out to observe changes in the Raman spectra depending on the laser output power, the acquisition time, and the objective lens. The qualification procedure focused on the most heat-sensitive material, uranium dioxide UO_2.

3.1.1. Effect of laser power on oxidation of UO_2

At the maximum power, P_{max}, without the attenuation filter, the laser beam significantly affected the UO_2 surface (white square in Fig. 3). At the minimum power with an attenuation filter in the laser beam (P_{min} + F3), optical images of another zone (red[1] square in Fig. 3) showed no effect after the same exposure time.

Fig. 4a is a typical Raman spectrum characteristic of the zone unaffected by the laser beam; Fig. 4b corresponds to the central zone of high-power laser beam impact (P_{max}). Both spectra (Fig. 4a and b) were obtained at low power (P_{min} + F3) to accurately identify the structural changes incurred by prior exposure of the UO_2 surface to the beam at P_{max} and P_{min} + F3. The spectrum in Fig. 4a shows three main peaks at 450, 575 and 1150 cm^{-1} characteristic of UO_2 and indicates no significant superficial changes at low power (P_{min} + F3). UO_2 has a fluorite structure with O_h symmetry, space group Fm-3m, and group theory predicts two vibration modes $T_{2g} + T_{1u}$. The first threefold degenerate vibration mode is only Raman-active (450 cm^{-1} in Fig. 4a) and the second only infrared-active [17]. The 575 cm^{-1} and 1150 cm^{-1} peaks in Fig. 4a have recently been assigned to 1LO and 2LO phonons. It must be remembered that although the origin of the 1150 cm^{-1} band is still debated in the literature [17–22], it is of interest to monitor this band as an indicator of the extent of UO_2 oxidation. Its intensity drops considerably for minor differences in stoichiometry [17]. The Raman spectrum in Fig. 4b is completely different and can

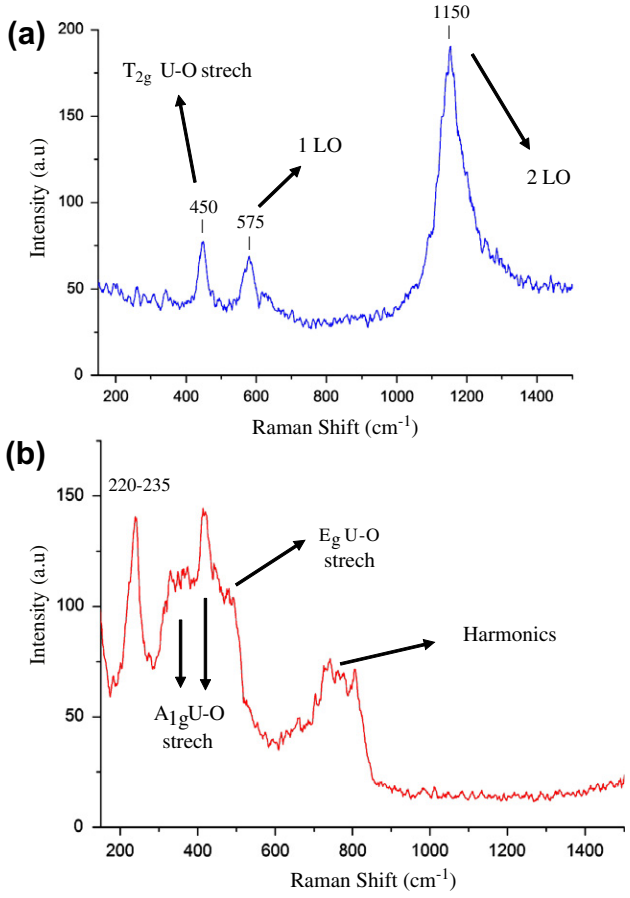

Fig. 4. (a) Characteristic UO_2 Raman spectrum at P_{min} + F3 without affecting the initial surface. (b) Characteristic α-U_3O_8 Raman spectrum at P_{min} + F3 following exposure at P_{max}.

[1] For interpretation of color in Figs. 1, and 3–12, the reader is referred to the web version of this article.

be attributed to a highly oxidized orthorhombic α-U_3O_8 [22–23]. The characteristic 1150 cm^{-1} peak of UO_2 has disappeared, and the 340, 405 and 480 cm^{-1} peaks are assigned to (U–O) symmetry changes affecting stretching modes A_{1g}, A_{1g} and E_g [17,22,23]. The band between 600 and 850 cm^{-1} is attributed to harmonics of the preceding modes. The 230 cm^{-1} peak remains uncertain, but was already clearly observed in previous studies [17,22,23] of α-U_3O_8. The appearance of an α-U_3O_8 phase also indicates that the local temperature at maximum power certainly exceeded 250 °C [12].

Raman mapping of the high-power (P_{max}) laser impact zone was performed under suitable low-power conditions (P_{min} + F3). The map in Fig. 3 covers an area of 10 × 10 μm^2 scanned in 0.5 μm steps. On this 3D image the *z*-axis plots the area variation for the 1150 cm^{-1} 2LO peak characteristic of UO_2 and observed only when highly oxidized compounds (O/U < 2.09) are not present [17]. The full-power laser beam clearly oxidized the UO_2 specimen surface, and the oxidized zone is sharply delimited. The two extreme situations shown here amply illustrate the importance of controlling the laser power, but also the possibility of using the beam as a local heat source to observe structural changes in actinide oxides.

3.1.2. Effect of spectrum acquisition time on oxidation of UO_2

Laser oxidation of UO_2 was also tested versus the exposure time and power level. Fig. 5 shows the intensity variations versus time for the 1150 cm^{-1} (UO_2) peak and for the 230 cm^{-1} peak associated with pronounced oxidation, at two laser power levels (P_{min} and P_{min} + F3). A Raman spectrum was recorded for 5 seconds at 5-s intervals with a total acquisition time of 30 min. Without the attenuation filter (red curves in Fig. 5), the 1150 cm^{-1} peak intensity diminished rapidly for 180 s, while the 230 cm^{-1} peak intensity increased slowly during the same time interval and then rose sharply to a plateau value. The slight increase in the 1150 cm^{-1} peak intensity after 180 s can be attributed to a change in the baseline due to the strong growth of the bands corresponding to the oxidized compound. When the filter was inserted immediately after laser (blue curves in Fig. 5) the intensity of both peaks remained constant over time and no change was observed on the beam impact surface. P_{min} + F3 is therefore favorable for determining spectrum changes after sample treatment without affecting the signal.

3.2. Characteristic low-power Raman spectra for actinide oxides $(U,Pu)O_2$

Fig. 6 compares the Raman spectra for the four materials examined. The spectra were acquired for 300 s at low laser power (P_{min} + F3) to prevent any effect on the beam impact surface.

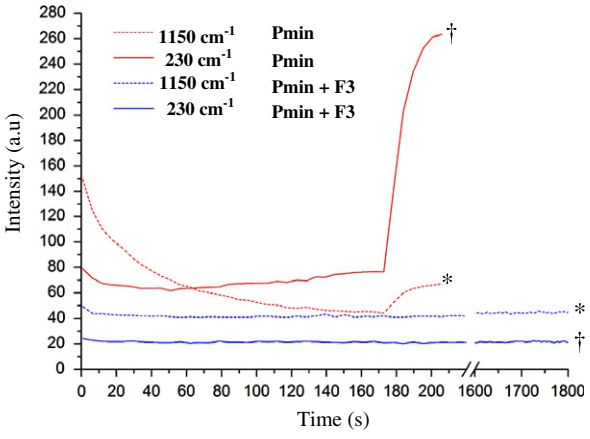

Fig. 5. Intensity of 1150 cm^{-1} (∗) and 230 cm^{-1} (†) peaks versus laser power (P_{min} or P_{min} + F3) and time for UO_2.

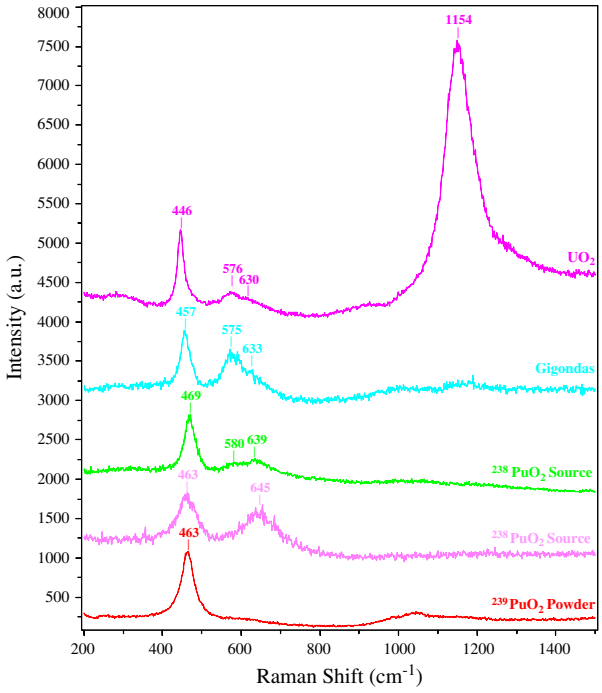

Fig. 6. Raman spectra of four experimental samples acquired over 300 s at low power (P_{min} + F3), not affecting the initial material surface under the beam.

It is interesting to note that the position of the T_{2g} Raman-active band for these fluorite structures (O_h symmetry) depends on the plutonium content. It is situated near 448 cm^{-1} (±2cm^{-1}) in the case of UO_2 and shifts toward higher wave numbers as the plutonium content increases in the solid solution: 457 cm^{-1} for the "Gigondas" samples (25 wt.% Pu) and 463 cm^{-1} or even 469 cm^{-1} for samples with high plutonium content. This can be interpreted by assuming a higher bond strength in PuO_2 than in UO_2 consistent with the shorter Pu–O bond length in the fluorite structure.

The spectrum region between 300 and 800 cm^{-1} is also very interesting to examine; a pseudo-Voigt function was used to deconvolute the spectrum (Figs. 7a and b). Regardless of the sample, two contributions were systematically observed beyond the T_{2g} peak: the first situated at 575–585 cm^{-1} and the second between 623 and 645 cm^{-1} depending on the sample.

He and Shoesmith [14] have recently shown that the relative intensities of these peaks for UO_2 depend to a large extent on the stoichiometry deviation. For significant stoichiometry deviations (UO_{2+x} where $x > 0.13$) the intensity of the 575 cm^{-1} (1LO) peak diminishes, while that of the 630 cm^{-1} peak increases and exceeds the 1LO peak [14,24]. The presence and coexistence of various defects (random point defects, Willis defect clusters, and mixtures of Willis and cuboctahedral defect clusters) [25–31] has been correlated with the relative intensity of these peaks in the lower uranium oxides (persistent fluorite structure, $x < 0.33$) [14]. For our UO_2 samples as well as for the "Gigondas" (25 wt.% Pu) sample, the largely predominant contribution of the 575 cm^{-1} 1LO peak (Fig. 7a) clearly indicates that these samples are near stoichiometric and does not suggest the presence of extended defects. In the case of UO_2 the high intensity of the 1153 cm^{-1} 2LO peak corroborates this conclusion (Fig. 6). For the "Gigondas" sample, breakdown in the selection rules caused by lattice damage can also contribute to the intense peak at 575 cm^{-1} [20].

The spectra for the samples with high plutonium content are also very instructive (Fig. 7b). For the lightly damaged $^{239}PuO_2$ powder the 580 cm^{-1} and 623 cm^{-1} peaks are of very low intensity compared with the very intense T_{2g} peak (Fig. 7b). Compare this result with the spectra obtained for the $^{238}PuO_2$ radioisotope

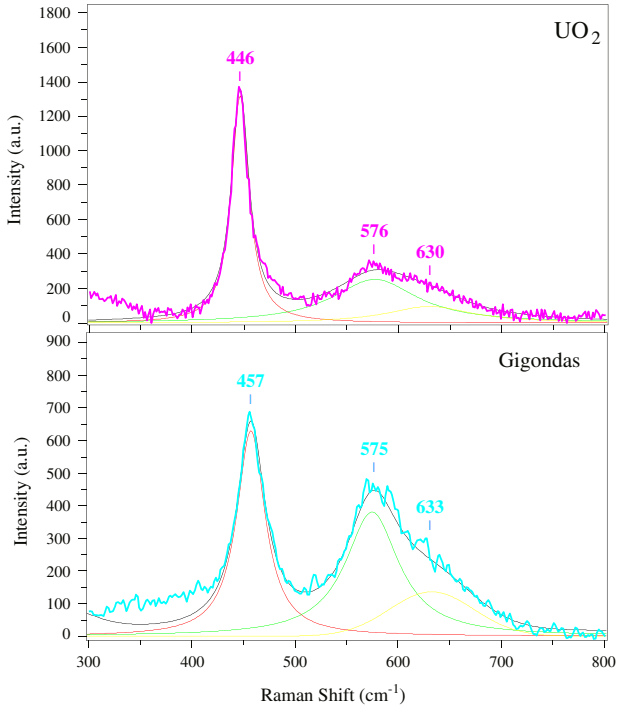

Fig. 7a. Deconvolution of peaks in 300–800 cm^{-1} region for UO_2 and "Gigondas" (25 wt.% Pu) samples. The spectra were acquired over 300 s at low power (P_{min} + F3), not affecting the initial material surface under the beam.

sources: two types of spectra were obtained for these sources (Figs. 6 and 7b) depending on the zone selected, with a very intense 645 cm^{-1} peak or sometimes two contributions at 579 and 639 cm^{-1}. The 579 cm^{-1} peak could be attributed to two sources by analogy with UO_2 [18,20]: the 1LO phonon frequency, or degenerate phonons found at similar energies but induced by disorder and irradiation. In each case the 639–645 cm^{-1} peak had the highest intensity after the T_{2g} peak, unlike the other lightly damaged samples. Two hypotheses account for the 639–645 cm^{-1} peak [18]:

- The formation of Frenkel pairs (vacancy and interstitial oxygen atom) on the anion sublattice is energetically very favorable [32–34] and could account for the high intensity of the 639 cm^{-1} peak compared with the undamaged sample [18].
- Uranium oxidation (the sample was severely damaged and contained about 20% ^{234}U produced by alpha decay) in the presence of air and alpha irradiation could occur over time in this porous sample and lead to the same kind of defect as in UO_2 without plutonium oxidation. A pure hyperstoichiometric UO_{2+x} structural defect signature cannot be excluded.

These observations raise the issue of the source (oxidation or irradiation) and nature of the defects ultimately with the possibility that similar defects can be formed in the fluorite structure in both cases. Raman spectra of a damaged Th(IV)O_2 fluorite structure would be very interesting to examine in order to discriminate between these effects. We have found Raman spectra of natural damaged thorianite (Belafeno origin, Malagasy Republic, RRUFF Database) showing a peak at 637 cm^{-1}, although unfortunately these natural samples also contain a few percent of uranium.

3.3. Resistance to laser-induced oxidation versus laser power and plutonium content

The behavior of the test samples subjected to the laser beam (local heating mode) was examined in order to deconvolute the

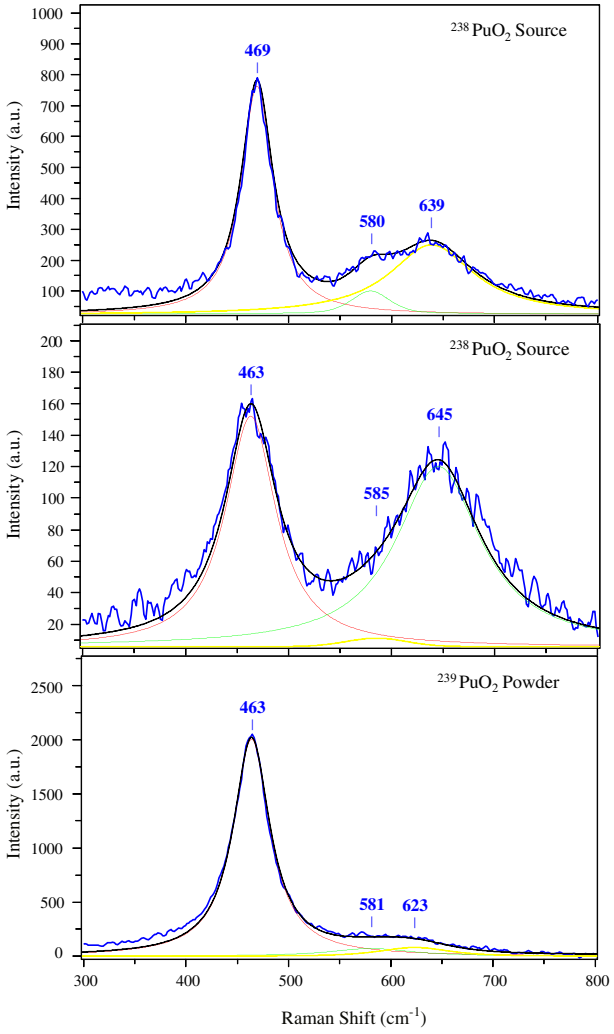

Fig. 7b. Deconvolution of peaks in 300–800 cm^{-1} region for $^{238/239}PuO_2$ samples. The spectra were acquired over 300 s at low power (P_{min} + F3), not affecting the initial material surface under the beam. For the $^{238}PuO_2$ source, two types of spectra were obtained.

effects of oxidation and irradiation damage on the Raman spectra.

Fig. 8 shows the Raman spectra versus time obtained for UO_2 and "Gigondas" samples at three different power settings: P_{min} + F3, P_{min}, and P_{min} + F3 after prior exposure at P_{max}. The beam exposure time was 300 s and the selected power levels allowed local heating gradually from P_{min} + F3 (no change expected: reference spectra) via P_{min} to P_{max}. Various zones and spots were selected on each sample to assess spectrum repeatability and determine the surface reactivity with respect to oxidation.

The material response to oxidation clearly depends on the plutonium content of the test oxide (Fig. 8). Significant UO_2 oxidation was observed after exposure to P_{max} and the Raman spectrum was characteristic of a higher oxide (α-U_3O_8) as discussed above. The effect on the "Gigondas" samples containing 25 wt.% plutonium was typified mainly by a higher-intensity 632 cm^{-1} peak and the disappearance of the at 575 cm^{-1} peak. These changes obviously correspond to a significant shift in the O/M ratio [14] but higher oxides (U_3O_8) were not observed in the "Gigondas" sample. This result demonstrates that plutonium is capable of limiting the oxidation of the fluorite structure in this mixed oxide compared with UO_2 as already noted in the literature [see the review in 35].

The Raman spectra for UO_2 at P_{min} also show significant oxidation under the laser beam, although it is important to note that ma-

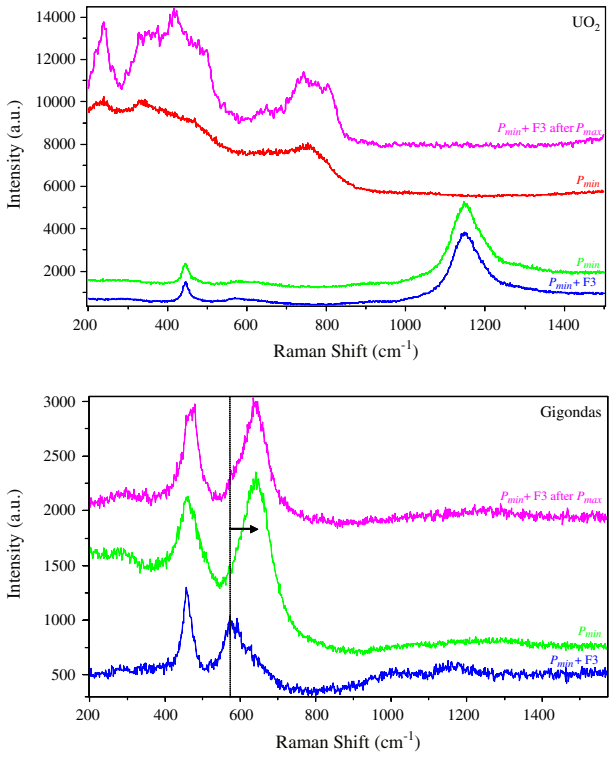

Fig. 8. Comparative oxidation resistance of UO_2 and "Gigondas" (25 wt.% Pu) samples versus laser power for identical exposure times (300 s) at P_{min} + F3, P_{min}, and P_{min} + F3 after exposure at P_{max}.

jor differences in oxidation reactivity were obtained depending on the grains probed (Fig. 9). Grains that appeared grayish under optical microscopy were oxidized more readily than lighter-colored grains, for which a UO_2 spectrum was conserved at P_{min}. Particular crystallographic orientations can account for such behavior [35] considering that the swelling due to the formation of higher oxides can occur along preferred directions that more readily accommodate structural changes (the reactivity follows the sequence [1 1 1] > [1 1 0] > [1 0 0]).

The "Gigondas" samples containing 25 wt.% Pu systematically exhibited lower reactivity than UO_2 with respect to oxidation after exposure at P_{max}. At lower power (P_{min}) the reactivity and oxidation kinetics of the UO_2 grains were highly variable for the same exposure time: in some cases no significant change in the spectra was observed compared with the UO_2 reference spectrum.

Fig. 10 illustrates the beam oxidation resistance of $^{238}PuO_2$ radioisotope sources over extended acquisition times (up to 300 s) at high power (P_{min} and P_{max}). Unlike the UO_2 and "Gigondas" (25 wt.% Pu) samples, no significant shift was observed in the spectra that might reflect changes in the crystallographic structural or additional defects due to oxidation under these severe beam exposure conditions. The 639 cm^{-1} peak was also very intense compared with the undamaged $^{239}PuO_2$ sample, and did not change when exposed to the laser beam. Assuming this peak reflects the presence of anion sublattice defects (Frenkel pairs), this implies that the local temperature under the beam was not sufficient to anneal them and therefore did not exceed 650 K [15]. Assuming this peak reflects the oxidation of uranium under long term interim storage in air; it is not surprising to not modify the spectra when the surface is exposed to the laser beam if the uranium was fully oxidized.

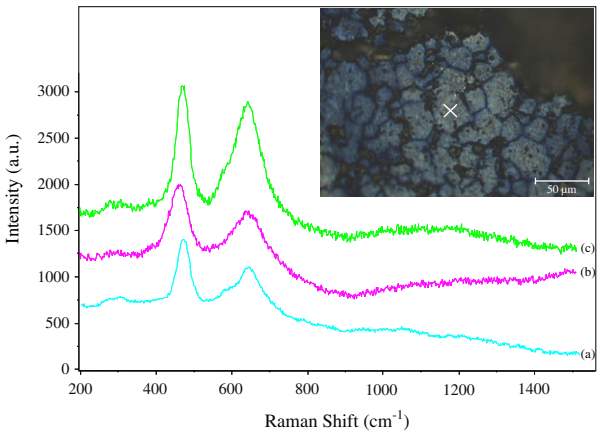

Fig. 10. Oxidation resistance in air of a radioisotope source ($^{238}PuO_2$) versus laser power: 30 s at P_{min} (a), followed by 300 s at P_{max} (b), and 40 s at P_{min} (c).

Spectra were also acquired on $^{239}PuO_2$ powder at P_{min} with the ×20 objective lens. Given the powder morphology, this sample could not be exposed to P_{max} without risking a strong interaction with the substrate. Fig. 11 very clearly shows the refinement of the Raman spectrum and especially the T_{2g} peak (enhanced aggregate crystallinity) when the powder was exposed to the beam, as well as a shift toward higher wave numbers (463–475 cm^{-1}). Two low-intensity peaks also appeared at 580 cm^{-1} and 1160 cm^{-1} after exposure to the beam (inset in Fig. 11) and can be assigned to the 1LO and 2LO vibration modes by analogy with stoichiometric UO_2. Beam exposure therefore does not lead to structural changes in $^{239}PuO_2$ powder under these experimental conditions.

3.4. Effect of water and hydrogen peroxide on the Raman spectra of $^{238}PuO_2$ radioisotope sources

It is important to evaluate the behavior of $(U,Pu)O_2$ solid solutions in contact with water, radiolysis products such as H_2O_2, and defects in the solid from the perspective, for example, of underwater interim storage of MOX fuel. Jégou et al. [11] recently

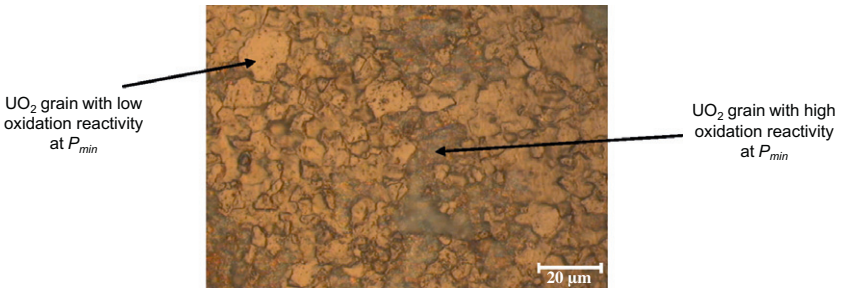

Fig. 9. Optical micrograph (×100) of UO_2 surface. Gray grains exhibit very strong oxidation reactivity at P_{min} compared with lighter grains.

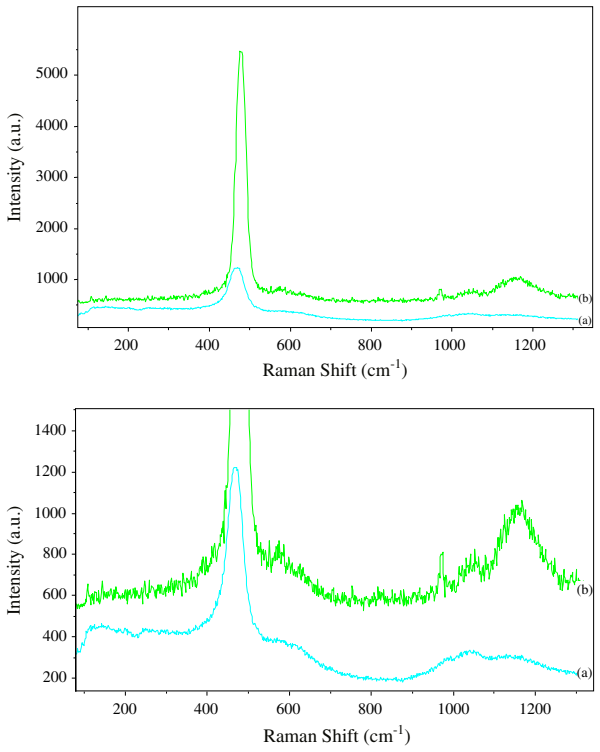

Fig. 11. Oxidation resistance in air of a $^{239}PuO_2$ powder versus laser power: (a) initial spectrum at P_{min} + F3; (b) spectrum at P_{min} + F3 after exposure of the powder at P_{min}.

showed that gamma radiolysis of water (10^{-4} M H_2O_2) resulted in very limited oxidation of aggregates containing 15–20 wt.% Pu compared with UO_2. However, the Raman spectra of aggregates altered in water showed a sharp increase in the intensity of the 638 cm^{-1} peak compared with the 580–585 cm^{-1} peak [11]. This behavior in water at 25 °C is very similar to that observed in this study for the "Gigondas" (25 wt.% Pu) samples during a oxidation in air under a laser beam (Fig. 8). We attempted to reproduce these phenomena in $^{238}PuO_2$ radioisotope sources heavily damaged in water and hydrogen peroxide (10^{-2} M H_2O_2). As the experiments in air had revealed no reactivity at any power level for this oxide, the power was arbitrarily set to P_{min}. This Raman spectra obtained are shown in Fig. 12. Remarkably, unlike the results obtained in air, a significant evolution was observed this time in the Raman spectra. First of all the 585 cm^{-1} peak intensity diminished in favor of the 638 cm^{-1} peak, as already observed by Jégou et al. [11]. Well defined new peaks appeared at 280, 330, 730 and 978 cm^{-1}, but

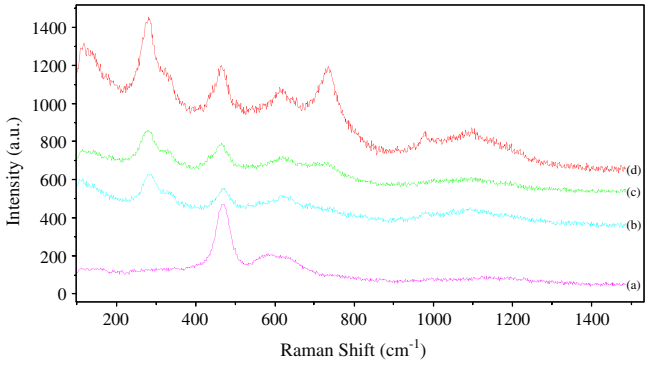

Fig. 12. Raman spectra for a radioisotope source in contact with water and H_2O_2: (a) 40 s at P_{min}; (b) 40 s at P_{min} + deionized water; (c) 40 s at P_{min} + H_2O_2 (10^{-2} M); (d) 100 s at P_{min} + H_2O_2 (10^{-2} M).

are difficult to identify at this time; it is possible that new uranium and plutonium compounds (peroxides, hydroxides, etc.) were formed [3–5,36–39]. The issue of plutonium oxidation remains uncertain. Calculations [2] have shown that PuO_2 oxidation by H_2O_2 could be energetically favorable with the formation of Pu_4O_9 as an intermediate reaction product on the oxide surface. Calculations [3] have also shown that the most stable oxidation product of PuO_2 could be $Pu_4O_8(OH)_2$ due in the change of the band structure induced by hydrogen. In any event they cannot be uranium peroxides (studtite and metastudtite), which have vibration modes at 820, 830 and 870 cm^{-1} [11,36,37]. These results reported here for the first time highlight a very specific behavior of $(U,Pu)O_2$/water interfaces subjected to irradiation and high laser power density.

4. Conclusions and outlook

This study demonstrates the interest of Raman spectroscopy for investigating the oxidation resistance of $(U_{1-y}Pu_y)O_2$ actinide oxides under various conditions. This original experimental approach consisted first in qualifying the experimental setup under the spectrum acquisition conditions, then using the laser beam as a local heat source to assess the reactivity and structural changes on the surfaces examined.

Structural changes in four materials $(U_{1-y}Pu_y)O_2$ with very different plutonium concentrations ($0 \leqslant y \leqslant 1$) and damage levels (up to 110 dpa) were studied by Raman spectroscopy to deconvolute the chemical and irradiation effects.

As expected, the oxidation resistance of these materials in air is highly dependent on their plutonium content. At the highest power levels (P_{max} and P_{min}) U_3O_8 generally forms with UO_2 whereas no significant change in the spectra indicating oxidation is observed for samples with high plutonium content. Samples containing 25 wt.% plutonium exhibit intermediate behavior, typified mainly by a higher-intensity 632 cm^{-1} peak and the disappearance of the 1LO peak at 575 cm^{-1}. This behavior can be attributed to the presence of anion sublattice defects without any formation of higher oxides.

At low power (P_{min} + F3) no shift was observed in the spectra exposed to the laser beam, making it possible to collect data on the intrinsic properties of the initial material. Under these conditions a high-amplitude peak at 639–645 cm^{-1} is clearly visible in heavily damaged materials (sample $^{238}PuO_2$). Two hypotheses could account for the 639–645 cm^{-1} peak. The formation of Frenkel pairs (vacancy and interstitial oxygen atom) on the anion sublattice is energetically very favorable and could account for the high intensity of the 639 cm^{-1} peak compared with the undamaged sample. Total uranium oxidation (the sample was severely damaged and contained about 20% ^{234}U produced by alpha decay) in the presence of air and alpha irradiation could occur over time in this porous sample and lead to the same kind of defect as in UO_2 without plutonium oxidation. A pure hyperstoichiometric UO_{2+x} structural defect signature cannot be excluded. Ideally it will be very interesting to study a fresh $^{239}PuO_2$ sample before and after a heavy ion bombardment. In practice a study performed with pure ThO_2 is certainly the best option to determine the evolution of Raman spectra before and after heavy ion bombardment without any oxidation of the fluorite structure.

The results obtained with water and hydrogen peroxide (a water radiolysis product) on a severely damaged $^{238}PuO_2$ specimen are important. Unlike the results obtained in air, a significant evolution was observed here in the Raman spectra. The 585 cm^{-1} peak intensity diminished in favor of the 638 cm^{-1} peak, as already observed by Jégou et al [11], and distinct new peaks appeared at 280, 330, 730 and 978 cm^{-1}, although it is difficult to assign them at

this time. These results highlight the importance of pursuing these studies in combination with other characterization techniques.

Acknowledgments

This study was carried out under the PRECCI research program funded jointly by the CEA and EDF. The authors are grateful to the DHA colleagues and to the personnel of Atalante for their technical support.

References

[1] J.M. Haschke et al., Science 287 (2000) 285.
[2] P.A. Korzhavyi et al., Nat. Mater. 3 (2004) 225–228.
[3] D.A. Andersson et al., Phys. Rev. B 79 (2009) 024110-1.
[4] S.D. Conradson et al., J. Am. Chem. Soc. 126 (41) (2004) 13443–13458.
[5] S.D. Conradson et al., J. Solid State Chem. 178 (2005) 521–535.
[6] P. Martin et al., J. Nucl. Mater. 320 (2003) 138–141.
[7] R. Guillaumont et al., Chemical Thermodynamics 5, OECD, 2003.
[8] P. Vitorge et al., J. Nuclear Soc. Technol. 3 (Suppl.) (2002) 713–716.
[9] V. Neck et al., J. Alloys. Comp. 444–445 (2007) 464–469.
[10] V. Neck et al., Radiochim. Acta. 95 (2007) 193–207.
[11] C. Jégou et al., J. Nucl. Mater. 399 (2010) 68–80.
[12] G.C. Allen et al., J. Nucl. Mater. 144 (1987) 17–19.
[13] J.R. Schoonover et al., Appl. Spectrosc. 54 (2000) 1362–1371.
[14] H. He, D. Shoesmith, Phys. Chem. Chem. Phys. 12 (2010) 8108–8117.
[15] D. Staicu et al., J. Nucl. Mater. 397 (2010) 8–18.
[16] R. Boucher, Y. Quere, J. Nucl. Mater. 100 (1981) 132–136.
[17] D. Manara, B. Renker, J. Nucl. Mater. 321 (2003) 233–237.
[18] T. Livneh, E. Sterer, Phys. Rev. B 73 (2006) 085118-1.
[19] J. Schoenes, J. Chem. Soc., Faraday Trans. 2 (83) (1987) 1205–1213.
[20] P.R. Graves, Appl. Spectrosc. 44 (1990) 1665–1667.
[21] S.D. Senanayake, H. Idriss, Surf. Sci. 563 (2004) 135.
[22] S.D. Senanayake et al., J. Nucl. Mater. 342 (2005) 179–187.
[23] M. Luisa Palacios, S.H. Taylor, Appl. Spectrosc. 54 (2000) 1372–1377.
[24] H. He et al., Electrochem. Commun. 11 (2009) 1724–1727.
[25] B.T.M. Willis, J. Phys. (Paris) 25 (1964) 431–439.
[26] B.T.M. Willis, Acta Crystallogr. A: Found. Crystallogr. A34 (1978) 88–90.
[27] F. Garrido et al., J. Nucl. Mater. 322 (2003) 87–89.
[28] C.R.A. Catlow, Proc. Royal Soc. London, Ser. A 353 (1977) 533–561.
[29] G.C. Allen, P.A. Tempest, Proc. Royal Soc. London, Ser. A 406 (1986) 325–344.
[30] D.J.M. Bevan et al., J. Solid State Chem. 61 (1986) 1–7.
[31] L. Desgranges et al., Inorg. Chem. 48 (2009) 7585–7592.
[32] M. Freyss et al., J. Nucl. Mater. 347 (2005) 45–51.
[33] J.P. Crocombette et al., Phys. Rev. B 64 (2001) 104107–104112.
[34] C. Meis, A. Chartier, J. Nucl. Mater. 341 (2005) 25–30.
[35] R.J. McEachern, P. Taylor, J. Nucl. Mater. 254 (1998) 87–121.
[36] M. Amme et al., J. Nucl. Mater. 306 (2002) 202–212.
[37] S. Bastians et al., J. Raman Spectrosc. 35 (2004) 726.
[38] V.P. Shilov et al., Radiochemistry 38 (1996) 217–219.
[39] J.M. Cleveland, The Chemistry of Plutonium, American Nuclear Society, 1979.